Biomaterials Science

Engineered coiled-coil HIF1α protein domain mimic

Journal:	*Biomaterials Science*
Manuscript ID	BM-ART-03-2024-000354.R1
Article Type:	Paper
Date Submitted by the Author:	02-Apr-2024
Complete List of Authors:	Britton, Dustin; NYU Tandon School of Engineering, Chemical and Biomolecular Engineering Katsara, Olga; NYU Grossman School of Medicine Mishkit, Orin; NYU Langone Health Wang, Andrew; NYU Tandon School of Engineering, Chemical and Biomolecular Engineering Pandya, Neelam; NYU Grossman School of Medicine Liu, Chengliang; New York University, Chemical and Biomolecular Engineering Mao, Heather; NYU Tandon School of Engineering, Chemical and Biomolecular Engineering Legocki, Jakub; NYU Tandon School of Engineering, Chemical and Biomolecular Engineering Jia, Sihan; NYU Tandon School of Engineering, Chemical and Biomolecular Engineering Xiao, Yingxin; NYU Tandon School of Engineering, Chemical and Biomolecular Engineering Aristizabal, Orlando; NYU Grossman School of Medicine Paul, Deven; NYU Tandon School of Engineering, Chemical and Biomolecular Engineering Deng, Yan; NYU Grossman School of Medicine Schneider, Robert; NYU Grossman School of Medicine Wadghiri, Youssef; NYU Langone Health Montclare, Jin; NYU Tandon School of Engineering, Chemical and Biomolecular Engineering; New York University, Chemistry

SCHOLARONE™
Manuscripts

Please do not adjust margins

ARTICLE

Engineered coiled-coil HIF1α protein domain mimic

Dustin Britton[a], Olga Katsara[b], Orin Mishkit[c,d], Andrew Wang[a,e,f], Neelam Pandya[c,d], Chengliang Liu[a], Heather Mao[a,c,d], Jakub Legocki[a], Sihan Jia[a], Yingxin Xiao[a], Orlando Aristizabal[c,d], Deven Paul[a], Yan Deng[g], Robert Schneider[b,h], Youssef Z. Wadghiri[c,d], and Jin Kim Montclare[a,c,i,j,k,*]

Received 00th January 20xx,
Accepted 00th January 20xx

DOI: 10.1039/x0xx00000x

The development of targeted anti-cancer therapeutics offers the potential for increased efficacy of drugs and diagnostics. Utilizing modalities agnostic to tumor type, such as the hypoxic tumor microenvironment (TME), may assist in the development of universal tumor targeting agents. The hypoxia-inducible factor (HIF), in particular HIF1, plays a key role in tumor adaptation to hypoxia, and inhibiting its interaction with p300 has been shown to provide therapeutic potential. Using a multivalent assembled protein (MAP) approach based on the self-assembly of the cartilage oligomeric matrix protein coiled-coil (COMPcc) domain fused to the critical residues of the C-terminal transactivation domain (CTAD) of the α subunit of HIF1 (HIF1α), we generate HIF1α-MAP (H-MAP). The resulting H-MAP demonstrates picomolar binding affinity to p300, the ability to downregulate hypoxia-inducible genes, and in vivo tumor targeting capability.

Introduction

Targeted cancer therapies often rely on passive targeting by leveraging the enhanced permeability and retention (EPR) effect or active targeting by exploiting overexpressed proteins in the tumor through specific complementary ligands displayed on a nanocarrier[1]. Active targeting, however, often suffers from several physiological/pathological pathways[2]. One route towards overcoming these pathways is to imbue nanomedicines with stimuli-responsiveness unique to tumor pathology, which may grant them with improved tumor release or retention[3].

One such feature of the tumor microenvironment (TME) that may be exploited is their naturally induced hypoxic environment due to disequilibrium between oxygen consumption[4]. Tumor survival is dependent on their ability to adapt to hypoxia, which is largely accomplished by activation of hypoxia-inducible factor (HIF), a transcription factor responsible for cellular homeostasis and inhibition of tumor suppressor genes[5]. The HIF isoform, HIF1 has been distinguished in cancer research due to its prevalence in tumors and is composed of a heterodimeric α and β subunit[5, 6]. The HIF1α subunit complexes with the co-activator protein p300/CREB binding protein (CPB) that generates a transcription factor to regulate expression during hypoxia[6].

Targeting of HIF1α/p300 has garnered interest yielding several peptides[7-12] designed to be a protein domain mimic (PDM) to HIF1α. Specifically, PDMs based on the C-terminal transactivation domain (C-TAD) of HIF1α (AA 786-826)[13-15] has exhibited specific binding and tumor targeting[14]. However, the short, unconstrained epitope of HIF1α C-TAD alone has been shown to be ineffective in downregulating hypoxia-inducible genes and is suspected to be proteolytically unstable due to its lack of helicity[13]. Using strategies to constrain a short peptide sequence of HIF1α to fix the helical secondary structure and expose critical residues has allowed for the generation of PDMs with nanomolar binding affinities[12, 14]. Commercial monoclonal antibodies generally possess binding affinities of 10 to 200 pM[16], leaving some avidity to be desired for current HIF1α PDMs [5]. Naturally, small peptide sequences with improved binding affinity have been of interest toward the development of protein-based targeting agents.

Recently, we have established the use of a multivalent assembled protein (MAP) as a PDM against the SARS-CoV-2 receptor binding domain (RBD) by using the cartilage oligomeric matrix protein coiled-coil (COMPcc or C) domain as a fusion scaffold with the N-terminal α-helix of the ACE2 receptor (ACE_{BINDER})[17], where entry of the virus is mediated[18]. C and ACE_{BINDER} are separated by a rigid kinked linker to offer improved solvent exposure resulting in ACE-MAP[17]. ACE-MAP exhibits the ability to self-assemble into a pentamer, offers high thermostability and improved binding affinity to the native ACE2 protein.

Using this approach, we use the 9 critical residues identified in the HIF1α C-TAD in previous PDMs[14] and graft to the C-terminus of ACE-MAP to generate HIF1α-MAPs (H-MAPs). The H-MAP helical scaffolds result in picomolar binding affinities, nearly 400-fold stronger than HIF1α C-TAD. Overall, our studies suggest that H-MAPs can be implemented to specifically complex p300 at picomolar affinity for *in vivo* targeting and visualization in tumors where future exploration of higher dosage may yield potential for H-MAPs as therapeutic agents for tumors. At nanomolar concentrations, we

[a] *Department of Chemical and Biomolecular Engineering, New York University Tandon School of Engineering, Brooklyn, New York, 11201, USA.*
[b] *Department of Microbiology, New York University School of Medicine, New York, New York, 10016, USA*
[c] *Center for Advanced Imaging Innovation and Research (CAI2R), New York University School of Medicine, New York, New York, 10016, USA*
[d] *Bernard and Irene Schwartz Center for Biomedical Imaging, Department of Radiology, New York University School of Medicine, New York, New York, 10016, USA*
[e] *Department of Biomedical Engineering, State University of New York Downstate Medical Center, Brooklyn, New York, 11203, USA*
[f] *College of Medicine, State University of New York Downstate Medical Center, Brooklyn, New York, 11203, USA*
[g] *Microscopy Laboratory, New York University Langone Health, New York, NY, 10016, USA*
[h] *Department of Radiation Oncology, New York University School of Medicine, New York, New York, 10016, USA*
[i] *Department of Chemistry, New York University, New York, New York, 10012, USA*
[j] *Department of Biomaterials, New York University College of Dentistry, New York, New York, 10010, USA*
[k] *Department of Biomedical Engineering, New York University, New York, NY, 11201, USA*
* *Corresponding author*

Electronic Supplementary Information (ESI) available: [Figures of H-MAP and H-MAP-N biosynthesis, ELISA curves for HIF1α C-TAD and COMpcc to p300, luciferase activity of Luc-MDA-MB-231 in normoxic and hypoxic conditions after incubation of COMPcc, preliminary NIR fluorescence of tumors ex vivo after injection of COMPcc, H-MAP-N, or saline at 500 nM protein concentrations, NIR fluorescence in vivo and measured total flux and radiance of tumors after injection of NIR-tagged COMPcc, H-MAP, and H-MAP-N, and tables for secondary structure compositions by CD and average mean area fluorescence for mouse organs ex vivo after injection of H-MAP-N and COMPcc]. See DOI: 10.1039/x0xx00000x

Please do not adjust margins

show the ability for H-MAP to specifically target p300 *in vitro* and target hypoxic tumors *in vivo*.

Materials and Methods

Materials

Chemically competent M15MA *E. coli* cells were gifted from David Tirrell at California Institute of Technology. H-MAP/pQE60 and H-MAP-N/pQE60 plasmid were cloned and purchased from Genscript. Bacto-tryptone, sodium chloride, yeast extract, tryptic soy agar, ampicillin, chloramphenicol, sodium phosphate dibasic anhydrous (Na_2HPO_4), sodium hydroxide (NaOH), dextrose monohydrate (D-glucose), magnesium sulfate, calcium chloride ($CaCl_2$), manganese chloride tetrahydrate ($MnCl_2{\cdot}4H_2O$), cobaltous chloride hexahydrate ($CoCl_2{\cdot}6H_2O$), isopropyl β-D-1-thiogalactopyranoside (IPTG), Pierce bicinchoninic acid (BCA) assay kit, Pierce snakeskin dialysis tubing 3.5 K MWCO, sodium dodecyl sulfate, Immulon 4 HBX ninety-six well plates, Nunc ninety-six well plates, Dulbecco's Modified Eagle medium (DMEM), gentamicin, µ-slide well glass bottom slides (ibidi), paraformaldehyde, Nunc EasYFlask Cell Culture Flasks, and ELISA wash buffer (30X) were acquired from Thermo Fisher Scientific. The twenty naturally occurring amino acids, thiamine hydrochloride (vitamin B), dimethylsulfoxide (DMSO), and 3,3',5,5'-tetramethylbenzidine (TMB) were purchased from Sigma Aldrich. Hydrochloric acid (HCl), Coomassie® Brilliant Blue G-250, and milk powder (non-fat, skimmed) were purchased from VWR. HiTrap Q HP 5 mL columns for protein purification were purchased from GE Healthcare Life Sciences. Macrosep and Microsep Advance Centrifugal Devices 3K molecular weight cutoff (MWCO) and 0.2 µm syringe filters were purchased from PALL. Acrylamide/bis solution (30%) 29:1 and natural polypeptide sodium dodecyl sulphate–polyacrylamide gel electrophoresis (SDS-PAGE) standard were purchased from Bio-Rad, pMD2G and psPAX2 plasmids, and HRE-Luciferase plasmid (#26731) were purchased from Addgene. p300 and Fugene6 were purchased from Promega. HIF1α protein was purchased from Abcam. IVISense 680 NHS Fluorescent Dye (VivoTag) was purchased from PerkinElmer.

Methods

Protein Modeling. Models for H-MAP solvent exposure were generated using Rosetta[19] and visualized in PyMOL[20]. A chain of the ACE-MAP PDB generated previously[17] was mutated in PyMOL after aligning the critical leucine residues in the HIF1α C-TAD with the critical ACE_{BINDER} residues in ACE-MAP as determined by Lan *et al.*[21]. Rosetta Symmetry protocol[22] using symmetry defined from pdb:3V2P and FastRelax protocols with the REF2015 score function[23] were used to generate 200 poses and the top scoring pose was used as the model for H-MAP. H-MAP was further refined for increased solvent exposure by removing two alanines in the rigid linker section of the sequence and generating 200 poses using the Symmetry[22] and FastRelax protocols with the REF2015 score function[23] and using the best scoring pose.

Expression and Purification. COMPcc was expressed and purified as previously described[24]. H-MAP/pQE60 and H-MAP-N/pQE60 were cloned and purchased from Genscript. Both plasmids were transformed into chemically competent M15MA cells that were gifted by David Tirrell. Transformed cells were plated onto agar plates with ampicillin (200 µg/mL) and kanamycin (35 µg/mL), and allowed to grow overnight at 37 °C. Colonies were selected and inoculated in starter cultures comprising of 16 mL minimal M9 media (0.5 M Na_2HPO_4, 0.22 M KH_2PO_4, 0.08 M NaCl, and 0.18 M NH_4Cl) containing all 20 canonical amino acids (100 µg/mL), ampicillin (200 µg/mL), kanamycin (35 µg/mL), vitamin B (35 µg/mL), D-glucose (100 µg/mL), magnesium sulfate (1 mM), and calcium chloride (0.1 mM). Starter cultures were added to a final volume of 400 mL minimal M9 media and grown at 37 °C and 300 rpm until an optical density at 600 nm (OD_{600}) of 0.8-1.0 was reached where 400 µL of 200 mg/mL IPTG was used to induce protein expression for 3 h at 37 °C and 300 rpm. Expression media was harvested by centrifugation at 5,000 × g for 20 min at 4 °C.

Cell pellets were resuspended in 40 mL Buffer A (50 mM TrisHCl, 250 mM NaCl, pH 8.0) and lysed by sonication via Q500 probe sonicator (QSonica) at 65% amplitude, 5 s on and 5 s off, for 2 min. Lysate was recovered by centrifugation at 11,000 × g for 50 min and flowing through a HiTrap Q High Performance 5 mL column (GE Health Sciences) charged with $CoCl_2$. Protein was washed and eluted using the following concentrations of imidazole (0 mM, 5 mM, 10 mM, 20 mM, 50 mM, 100 mM, 200 mM, 500 mM) added to Buffer A. Pure elutions were confirmed by 12% SDS-PAGE (**Figure S1a**, **S2a**). Elutions containing 50-200 mM imidazole were collected and dialyzed in 3.5 kDa MWCO tubing membrane overnight in a 5 L bucket of Buffer A. Following, dialyzed protein was concentrated in a 3 kDa centrifugal Macrosep and Microsep Advance centrifugal filters (Pall Corporation) until a final volume of 1.5 mL was reached before being injected with successive 500 µL samples into a Fast Purification Liquid Chromatography (FPLC, AKTA pure, GE healthcare) system equipped with a Superdex 75 10/300 GL Size Exclusion Chromatography (SEC) column and eluted with phosphate buffered saline (PBS) pH 7.4 (**Figure S1b, S2b**). Pure fractions were confirmed by 12% SDS-PAGE (**Figure S1c, S2c**). Pure fractions were collected between 14-24 mL and further concentrated using 3 kDa centrifugal Microsep Advance centrifugal filters (Pall Corporation). Pure fractions were confirmed by 12% SDS-PAGE and protein concentration was determined using a bicinchoninic acid (BCA) assay with a standard curve from serial dilutions of bovine serum albumin.

Circular Dichroism Spectroscopy. H-MAP and H-MAP-N secondary structure was assessed on a Jasco J-815 circular dichroism (CD) spectrometer equipped with a PTC-423 single position Peltier temperature control system. Wavelength scans were performed at room temperature from 190 to 250 nm using 1 nm step sizes for 10 µM protein in PBS pH 7.4. Temperature scans were performed from 25 °C to 85 °C at 10 µM in PBS pH 7.4 using 1 °C step size at 10 µM protein concentration. Mean residue ellipticity (MRE) was calculated as previously described[25] and Savitzky-Golay smoothening was applied using Spectra Analysis software (version 1.53.04, JASCO Corporation).

Cell Culture. Human MDA-MB-231 cells (231, cat#CRM-HTB-26/RRID:CVCL_006) and murine 4T1 cells (cat#CRL-3407/RRID:CVCL_GR31) were purchased from ATCC and maintained as previously described; 4T1-Luc cells were created by infecting cells using packed lentiviral particles of mCherry-eFFLy Luciferase (cat#104833, Addgene) as previously described[26].

Cytotoxicity Assay. Triple negative human breast cancer (TNBC) MDA-MB-231 and Luc-MDA-MB-231 cell lines were incubated in DMEM media (Thermofisher) supplemented with 10% fetal bovine serum (FBS) albumin. Adherent MDA-MB-231 cells were grown to 70-80% confluence in a flask incubated at 37 ºC. 10,000 cells/well were seeded onto a clear 96-well plate in 100 µL DMEM supplemented with 10% FBS and incubated at 37 °C with 5% CO_2 overnight. DMEM was subsequently removed, and wells were incubated with dilution of H-MAP-N in PBS for 24 and 48 h at 37 °C with 5% CO_2. MTT (3-(4,5-dimethylthiazol-2-yl)-2,5-diphenyltetrazolium bromide) cell viability assays were then conducted on the wells. The absorbance of each well was assessed using a Biotek Synergy HT microplate reader at 540 nm. Cell viability was then calculated by normalizing to untreated (PBS only) cell controls. Average and standard deviation was calculated using three sample incubation trials.

Fluorescent labeling. H-MAP, H-MAP-N, and COMPcc proteins were conjugated to VivoTag by NHS ester reaction at phosphate buffer, PB, (50 mM Na_2HPO_4 pH 8.0) by mixing at 10:1 VivoTag:protein ratio and incubation for 6 h at RT and 300 rpm. The reaction was quenched by dialysis in PB overnight. VivoTag-labelled protein was separated from excess dye by affinity chromatography purification using HiTrap Q High Performance 5 mL column (GE Health Sciences) charged with $NiSO_4$. Pure protein was eluted using increasing concentrations of imidazole (0 – 1 M) and confirmed by 12% SDS-PAGE. Pure elutions were collected and dialyzed using 3.5 kDa MWCO membrane tubing in three 5 L buckets of PB. Protein was subsequently concentrated using Microsep Advance centrifugal filters (Pall Corporation). Labeling percentage was measured by using a standard curve of VivoTag compared to protein concentration measured by BCA assay. 1 µM stock concentrations were made by normalizing to the relative fluorescence based on relative labeling.

Cell Uptake and Microscopy. Cells were seeded onto a µ-Slide 8 well glass bottom plate with #1.5 cover slip (ibidi) overnight at 37 °C and 5% CO_2 in 300

This journal is © The Royal Society of Chemistry 20xx

µL DMEM media supplemented with 10% FBS. Media was subsequently removed and replaced with 300 µL fresh media containing 0 or 100 nM final concentration of H-MAP and H-MAP-N protein labeled with VivoTag and incubated for 72 h at 37 °C and 5% CO_2. Following, media was aspirated from the wells and incubated with 2% paraformaldehyde (PFA) in PBS for 20 min at 37 °C and 5% CO_2. The wells were then aspirated and washed with Dulbecco's PBS (DPBS, Gibco) and stored in 300 µL media at 4 °C until examination with the microscope. Regions of interest (ROIs) of cell nuclei were assessed in ImageJ for mean integrated intensity and compared.

Enzyme-linked immunosorbent assay (ELISA). The binding affinity of H-MAP, H-MAP-N, HIF1$\alpha_{786\text{-}826}$, and COMPcc to the p300 protein was assessed by ELISA. p300 peptide was purchased from Promega and diluted to 2 units/µL before plating 50 µL on a Immulon 4 HBX 96-well plate and storing at 4 °C overnight. Following, wells were aspirated and blocked with 100 µL/well of 3% non-fat milk prepared in PBS with 0.1% Tween 20 (TPBS) for 2 h at RT. Blocking solution was removed and replaced with 100 µL serial dilutions of H-MAP or H-MAP-N in TPBS with 1% non-fat milk for 1 h. Wells were then aspirated and washed three times with 1% non-fat milk in TPBS before being incubated with 100 µL of 1:3000 anti-Histag horseradish peroxidase (HRP) conjugated secondary antibody (Sino Biological) in TPBS. Plates were then washed three times with 1x ELISA wash buffer (Thermo Scientific) and allowed to dry for 20 min in a hood. TMB solution was then freshly prepared in DMSO at 1 mg/mL and added to 0.05 mM citrate-phosphate buffer with 0.01% hydrogen peroxide. 100 µL of TMB solution was added to the plates for approximately 10 min before being quenched with 50 µL of 3 M HCl. Absorbance at 450 nm was subsequently read using a Biotek Synergy HT microplate reader. Graphpad Prism nonlinear regression using the One site – Total Binding – Saturation Kinetics equation.

Luciferase Assay. The ability for H-MAP-N to downregulate hypoxia-inducible genes was assessed using MDA-MB-231-HRELuc cells using a luciferase assay. Briefly, 65,000 cells/well were seeded overnight onto a 24-well plate in 500 uL of DMEM media supplemented with 10% FBS at 37 °C and 5% CO_2. The next day cells were transfected using Fugene6 (Promega) according to the manufacturer's instructions with HRE-Luciferase plasmid (#26731, Addgene). The next morning, media was replaced and 0, 10, or 100 nM of H-MAP-N was added for 6 h. Cells studied under hypoxic conditions were then superficially induced for hypoxia by addition of $CoCl_2$ to a final concentration of 100 µM using a freshly prepared 20 mM $CoCl_2$ stock for 18 h at 37 °C and 5% CO_2. Cells were lysed using 1X lysis reagent (Cell Culture Lysis Reagent, Promega) and collected into chilled 1.5 mL Eppendorf tubes and centrifuged at 13,000 rpm for 10 min at 4 °C. 20 µL of cell lysate was mixed with 100 µL of luciferase assay reagent (Promega) and remaining sample was measured for protein concentration by BCA assay. Luminescence intensity was measured on a white 96-well plate using a Biotek Synergy HT microplate reader and normalized by protein concentration and maximum luminescence. Average and standard error are reported based on two independent trials.

***In vivo* and *ex vivo* Fluorescence imaging.** All studies were approved by the NYU Grossman School of Medicine Institutional Animal Care and Use Committee (IACUC) and conducted in accordance with IACUC guidelines. Female Balb/cJ mice (N=20), 6-8 weeks old (cat no: 000651) were purchased from Jackson Labs. All mice were injected orthotopically in the 4th mammary fat pad with 300,000 syngeneic 4T1-Luc mammary carcinoma cells (70:30 cell to Matrigel ratio (CAT:#356237)). Tumors were allowed to grow for two weeks until reaching a size of approximately ~100 mm^3. Preliminary studies assessed the fluorescence of H-MAP-N and COMPcc at 500 nM in 100 µL volume (as determined by BCA assay) in n=2 per group, injected retroorbitally. A saline (PBS) control treatment was used in one mouse to evaluate if significant tumor autofluorescence was present. In our follow-up study, 100 µL of H-MAP, H-MAP-N and COMPcc were injected retroorbitally at 1 µM concentration, normalized for VivoTag fluorescence at ex/em 630 nm/680 nm. Twenty minutes after injection, the lower body of mice were scanned *in vivo* using fluorescence imaging, while the rest of the body was covered with a black paper to minimize signal interference from autofluorescence, light scattering and diffusion. Primary tumors were then excised, and organs were collected and immediately imaged with the same scanner.

Fluorescence imaging was conducted using both *in vivo* and *ex vivo* using a Bruker Xtreme II Optical and X-ray small animal imaging system, commonly referred to as IVIS (*in vivo* imaging system). This system boasts high sensitivity for luminescence, fluorescence, radioisotopic and radiographic imaging. It is equipped with a back-illuminated 400W Xenon lamp and a 4MP CCD camera which is cooled to -90°C with a Peltier cooler. The setup operates on a novel inverted detection platform, ensuring uniform imaging by minimizing cross-sample shadowing, maintaining a consistent flat focal plane, and reducing the light path from the subject being imaged to the CCD camera.

Moreover, the entire detection system, including the CCD, lens, diopters, and emission filters is mounted on an elevator platform with 6 preset field-of-view positions (FOV: 7.2, 10, 12, 15, 18, 19 cm^2). This innovative design facilitates a seamless transition between *in vivo* whole-body imaging and *ex vivo* organ imaging. The system allows for high resolution imaging at a high zoom level and multi-animal imaging at low zoom level. Importantly, the system effortlessly shifts between imaging modalities without disturbing the positions of the examined animals, ensuring inherent multimodal image registration across all field of views (FOVs) for every modality.

For the *in vivo* imaging procedures, all animals were initially anesthetized for 3 to 5 minutes within an induction chamber using 3-5% isoflurane mixture in air at a flow rate of 1.5 L/min. Subsequently, the 5 animals were staged, and anesthesia was maintained under 1-1.5% isoflurane while being placed on a temperature-controlled stage. Imaging settings included a binning configuration of 4x4 and a field of view of 190 mm. Exposure time and f/stop – the relative size of the opening of the aperture – were optimized for either simultaneous *in vivo* imaging of 5 subjects or for *ex vivo* scanning of excised organs placed within a dish. The excitation and emission wavelengths were set to λ(ex) = 630 nm and emission λ(em) = 680 nm, respectively.

Image Analysis: Following image acquisition, all datasets were analyzed using the proprietary Bruker Molecular Imaging (BMI) software (version 7.5.3.22464). This software not only allows for controlling the acquisition process but also offers a range of tools for image preparation and data analysis. All images were presented in terms of fluorescence efficiency, defined as the ratio of the collected fluorescent intensity to an internal standard of incident intensity at the selected imaging configuration. Regions of interest (ROIs) were delineated around the site of tumor implantation, and ROI signal intensities were quantified in terms of fluorescent efficiency.

To provide a comprehensive understanding of the fluorescence characteristics of H-MAP, H-MAP-N, and COMPcc, their relative fluorescence intensity was quantified using both total flux and average radiance. This dual-parameter approach captures both the overall emitted photon quantity (total flux) and the radiative power per unit solid angle (average radiance), offering a more nuanced perspective than relying solely on one measure. This is particularly advantageous here, as it allows for not only directly comparing these materials but also facilitating comparison with prior studies that may report either total flux or average radiance.

Statistical Analysis. GraphPad Prism (GraphPad Software) was employed for statistical analysis using Student's unpaired *t*-test and one-way ANOVA.

Results and Discussion

Protein design. We have previously designed a multivalent assembled protein (MAP) by fusion of the N-terminal α-helix of the human cell receptor protein ACE2 for recognition of the RBD of SARS-COV-2 utilizing a kinked rigid linker to the COMPcc domain[17]. We utilized this protein sequence as the foundation of new MAPs for inhibition of the HIF1α•p300 complex (H-MAP) (**Figure 1a**). To do so the residues critical for recognition with the p300 complex were grafted onto solvent exposed residues of C-terminus of ACE-MAP (**Figure 1a**). Specifically, the sequence GEELLRALDQVN was substituted at the C-terminus for HEAEDLFYQS which allowed for residues critical for binding in the HIF1α•p300 complex, L818, L822, D823, and Q824[15] to have solvent exposure.

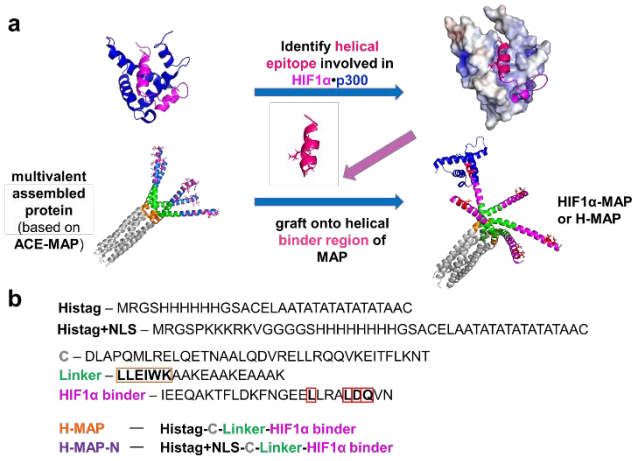

Figure 1 a. Schematic for H-MAP design strategy using PyMOL cartoons where the critical residues involved in HIF1α•p300 complex (pdb: 1L8C) are grafted onto MAP domain and linker domain optimization by computationally predicted increase in solvent exposure. **b.** Sequence order and configuration for H-MAP and H-MAP-N, which involves a histag domain followed by C, Linker, and HIF1α binder domains. H-MAP-N linker domain possesses additional NLS and G_4S linker sequence in this histag domain. Kinked region of the linker sequence is bolded and highlighted by the orange box and color in the pdb cartoon. Critical residues in the HIF1α•p300 for HIF1α-binding are bolded and highlighted by the orange box and color in the pdb cartoon.

Poses of the structure were confirmed to be similar to those produced for ACE-MAP[17] by using the Rosetta Relax[27] protocol and all-atom energy score function[23]. A sequence was first designed using the linker sequence used in ACE-MAP and another sequence with a shortened linker was designed in parallel to test the ability to improve protein structure and fit for therapeutic binder sequences (**Figure 1a**). To generate the H-MAP linker, Rosetta was used to test removal of non-critical residues in the kinked linker region to adjust the constellation of the solvent exposed residues and decrease the distance between the C domain and the binding domain in which an alanine was removed from the first two AAAK linker sequences. This also resulted in an improved overall Rosetta score and Rosetta score/amino acid (AA) from -1312 kcal/mol and -10.17 kcal/mol-AA to -1362 kcal/mol and -10.72 kcal/mol-AA for the ACE-MAP linker and H-MAP, respectively. The best scoring poses visualized in PyMOL[20] showed that the modified kinked linker in H-MAP provided an increased angle (from ~40° to ~70° assessed visually in PyMOL) and the helical pitch allowed the critical leucine residues to be pointed in a corresponding outwards direction, which maintained a high degree of solvent exposure. Furthermore, sufficient distance between p300 and H-MAPs were calculated in PyMOL where the distance from the center-of-mass from the C-terminus of the COMPcc domain to the center-of-mass of p300 after superposition was measured to be 5.4 nm. Without the adjustment in the linker from the previous ACE-MAP design, the distance would have been 6.0 nm. To demonstrate the H-MAP design to reduce the likelihood of steric hinderance of multivalent binding domains, the p300 domain was superimposed onto each arm and their distances between center-of-masses were calculated to be 5.5 nm, whereas without the adjustment in the linker from the previous ACE-MAP design, the distance would have been 4.7 nm (**Figure S3**).

H-MAP sequences were then synthesized with (H-MAP-N) and without (H-MAP) the addition of a nuclear localization sequence (NLS) comprising of sequence PKKKRKV inserted at the N-terminus followed by a flexible G_4S linker prior to the histidine tag (Histag) to facilitate localization near HIF-α subunits[28].

Structure and Binding. To assess structure, circular dichroism experiments were conducted (**Figure 2a**). H-MAP and H-MAP-N wavelength scans at 25 °C revealed a double minima characteristic of α-helical protein structures (**Figure 2a**). H-MAP possessed a double minima of -10,000 ± 2,000 deg•cm^2•dmol^{-1} at 208 nm and -9,400 ± 2,000 deg•cm^2•dmol^{-1} at 222 nm with a 222/208 of 1.0 ± 0.1 whereas H-MAP-N possessed a double minima of -9,800 ± 500 deg•cm^2•dmol^{-1} at 208 nm and -9,300 ± 900 at 222 nm with a 222/208 of 1.0 ± 0.1 (**Table S1**). The spectra similarity indicated that the NLS sequence in H-MAP-N had a negligible impact on the helical secondary structure. Prior MAP constructs possessed similarly high 222/208 ratios, suggesting α-helices to exist close together rather than alone [29-31] (**Table S1**). Spectra analysis *via* CONTIN software [32-34] (**Figure 2b, Table S1**) revealed H-MAP- and H-MAP-N both exhibited 36% α-helical content; there were very modest differences in the remaining conformations where H-MAP and H-MAP-N revealed 27% and 29% β-sheet content, and 37% and 35% random coil content, respectively.

When compared to ACE-MAP parent [17], both constructs exhibited slightly lower α-helical conformation, and slightly greater β-sheet and random coil content. Additionally, the matching secondary content by CONTIN also supported the negligible structural differences presented by addition of the NLS sequence in H-MAP-N. Overall, grafting of the HIF1α to ACE-MAP demonstrated structured confirmation affirming helicity. The HIF1α C-TAD is relatively unstructured and considered an intrinsically disordered protein alone[35]. Additionally, the binding domain in H-MAP is the result of engraftment onto the binding domain for another target (ACE2•SARS-CoV-2) which may be the cause for the relatively lower helicity exhibited in H-MAPs compared to ACE-MAPs[17, 36]. Future design of MAPs may benefit from studying the design of more universally favorable linker and binding sequences to accommodate the engraftment of a variety of short helical sequences such as HIF1α C-TAD. Additionally, the matching secondary content by CONTIN also supports the negligible structural differences presented by addition of the NLS sequence in H-MAP-N.

H-MAP and H-MAP-N also exhibited relatively high melting temperature (T_m) (**Figure 2a, Table S1**) of 66.6 ± 0.2 °C and 69.9 ± 1.7 °C, respectively. The presence of the NLS on H-MAP-N thus led to a slight increase in T_m relative to H-MAP. Interestingly, H-MAP and H-MAP-N presented statistically significant increases in thermostability over the parent ACE-MAP by 2.6 °C and 5.9 °C, respectively [17].

This journal is © The Royal Society of Chemistry 20xx

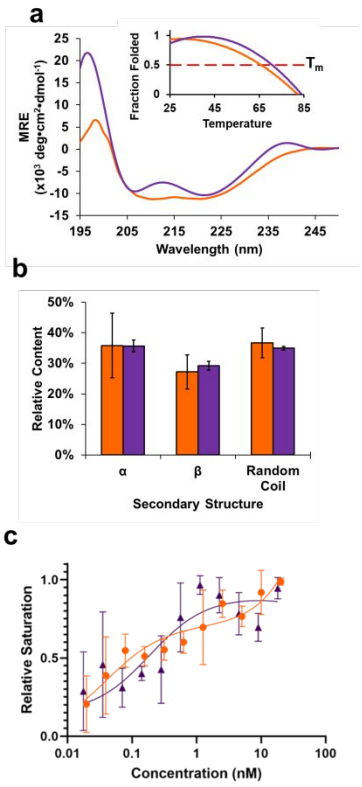

Figure 2 a. Average circular dichroism spectroscopy wavelength scans of H-MAP (orange) and H-MAP-N (purple) from 190 to 250 nm from three independent trials and polynomial fits of average temperature scans of H-MAP (orange) and H-MAP-N (purple) from two independent trials (inset) **b.** Average secondary structure content of H-MAP (orange) and H-MAP-N (purple) wavelength scans deconvoluted using CONTIN software where error bars represent the standard deviation from three independent trails. **c.** Binding of H-MAP (orange) and H-MAP-N (purple) to p300 measured by ELISA where error bars represent the standard deviation of three independent trials.

In order to determine affinity of H-MAP constructs to target p300, enzyme-linked immunosorbent assay (ELISA) was carried out (**Figure 2c**). Total binding saturation kinetics per monomeric unit of H-MAP were used to determine the average binding affinities (K_d) and their confidence intervals (CI) where H-MAP exhibited a K_d of 40.5 pM (18.0 – 106.1 pM @95%CI), and H-MAP-N possessed a K_d of 190.9 pM (35.8 – 642.5 pM @95%CI) (**Figure 2c**). The presence of the NLS in H-MAP-N resulted in a 4.7-fold loss in binding. Relative to HIF1α$_{786-826}$, which had a K_d of 14.5 nM (2.8 – 91 nM @95%CI) (**Figure S4a**), H-MAP and H-MAP-N showed a 358-fold and 76-fold improved affinity, respectively. As a negative control, COMPcc was assessed for binding to p300 and revealed no significant binding by ELISA (**Figure S4b**).

Cell Uptake and Cytotoxicity. As the HIF1α protein complexes with p300 in the nucleus, we investigated the cellular uptake of H-MAP proteins and COMPcc in triple-negative breast cancer (TNBC) cell line MDA-MB-231 (**Figure 3a-d**). H-MAP, H-MAP-N, and COMPcc were labeled a near-infrared (NIR) tag (VivoTag), purified, and incubated with MDA-MB-231 cells for 72 h and visualized *via* confocal microscopy using 630 nm/680 nm excitation/emission. Interestingly, we observed that cells treated with H-MAP or H-MAP-N exhibited an inhibition of cell proliferation (**Figure 3c-d**) compared to cells treated with PBS or COMPcc (**Figure 3a-b**). Moreover, while NIR-tagged COMPcc provided an observable increase in fluorescence inside cells compared to PBS, fluorescence was retained within the endoplasmic reticulum whereas H-MAP and H-MAP-N fluorescence was also observed in the nucleus. Of cell nuclei measured, 88% of H-MAP cell nuclei and 90% of H-MAP-N cell nuclei possessed increased fluorescence six standard deviations above the mean fluorescence observed in cells treated with PBS, whereas 0% of nuclei cells treated with COMPcc possessed such fluorescence. Using 2way ANOVA analysis in Prism (GraphPad), H-MAP and H-MAP-N samples exhibited cells with an increased fluorescence within the nucleus in comparison to cells incubated with phosphate buffered saline (PBS) or COMPcc alone (**Figure 3e**). Conversely, H-MAP and H-MAP-N did not exhibit significant differences between the cells (p-value 0.50). Overall, fluorescently tagged H-MAP constructs indicated that the protein is readily uptaken by the cells and were good candidates for targeting hypoxic environments such as those generated by tumors. Since structure, targeting, cell uptake, and *in vitro* domain recognition of H-MAP-N showed promise, it was selected for further *in vitro* studies.

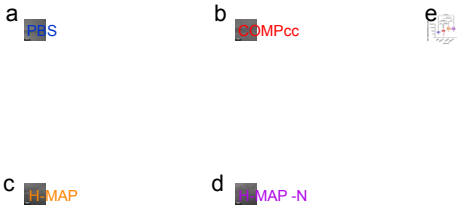

Figure 3 a-d. Representative confocal microscopy images of MDA-MB-231 cells incubated with phosphate buffered saline (PBS), COMPcc, H-MAP, and H-MAP-N using an overlay of brightfield and fluorescence using 490 nm excitation. **e.** Boxplot of mean integrated intensity of cell nuclei using representative regions of interest from confocal microscopy images of MDA-MB-231 cells with no protein, H-MAP, and H-MAP-N where error bars are the standard deviation of 50 independent cell nuclei. **** represents p-value < 0.0001.

To assess, for the ability to downregulate transcription of hypoxia-inducible genes, we employed MDA-MB-231 cell lines transfected with a hypoxia-induced luciferase gene (Luc-MDA-MB-231) as described previously[14]. H-MAP-N exhibited significant inhibition of hypoxia-induced luciferase by 10 nM (**Figure 4a**). This luciferase-based assay indicated the ability for H-MAP-N to downregulate hypoxia-induced genes serving as a promising tool for targeting tumor environments. In comparison, the negative control, COMPcc, showed negligible differences in the same concentration range on the ability to downregulate the Luc-MDA-MB-231 cell luciferase activity (**Figure S5**). H-MAP-N was also assessed for cytotoxicity in MDA-MB-231 cell line by MTT assay; there was no significant increases in cell toxicity at 24 h in the concentration range (≤ 100 nM) used for *in vitro* HIF1α/p300 inhibition (**Figure 4b**). However, H-MAP-N displayed a slight decreasing trend in cell viability in this concentration range, which became statistically significant at 100 nM indicating an upper limit.

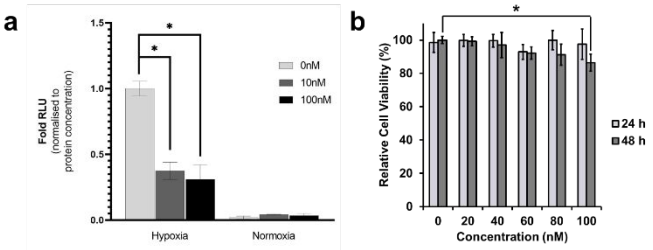

Figure 4 a. Transcriptional regulation of hypoxia-inducible genes by H-MAP-N by downregulation of hypoxia-induced promoter activity in relative luminescence units (RLU) from Luc-MDA-MB-231 cells under normoxic and hypoxic conditions. * represents p-value < 0.05, ** represents p-value <0.005 **b.** MTT cell viability assay for H-MAP-N at 24 h and 48 h incubation at 37 °C in MDA-MB-231 cells. * represents p-value < 0.05.

***In vivo* Tumor Localization and Biodistribution.** We administered COMPcc, H-MAP, and H-MAP-N to 4T1 TNBC xenograft mouse models. To effectively track the fate of our protein-based compounds, we conjugated a near-

infrared (NIR) tag (VivoTag) to all three compounds – H-MAP, H-MAP-N, and COMPcc, the latter for a comparable control. Separate groups of mice with TNBC tumors (n=10 total, n=5 for each group) received injections of all three compounds, each at 100 µL volume with a concentration of 1 µM normalized by effective fluorescence of VivoTag.

Ex vivo examination of fluorescent signals from extracted organs such as the tumor, liver, and kidneys revealed obvious differences at an excitation/emission wavelengths of 630/680 nm (**Figure 5a**). Upon comparing H-MAP and H-MAP-N to COMPcc, a statistically significant increase in total fluorescence from the tumor for both H-MAP and H-MAP-N was observed, indicating specific localization within the tumor (**Figure 5b-c, Table S2**). This specificity can be attributed to the high binding affinity and thermostability of H-MAP and H-MAP-N.

In summary, the capacity of H-MAP and H-MAP-N to accumulate specifically within the tumor *in vivo*, particularly evident in *ex vivo* imaging experiments at low concentrations, demonstrates the targeting ability and sensitivity to detect hypoxic TME. This is likely due to the significant increase in binding affinity in H-MAP and H-MAP-N to the picomolar range compared to previous domain mimics which had not yet previously achieved affinities better than the nanomolar binding affinity of native HIF1α C-TAD. In fact, many fluorescently conjugated antibodies typically report binding affinities in the nanomolar range[37-40]. Thus, H-MAPs, which are more facilely produced in *E. coli* and do not require post-translational modifications, present an alternative to fluorescently tagged antibodies. This potential extends to its use as an *in vivo* tumor diagnostic agent following radiolabeling, owing to its affinity for areas of increased local hypoxia.

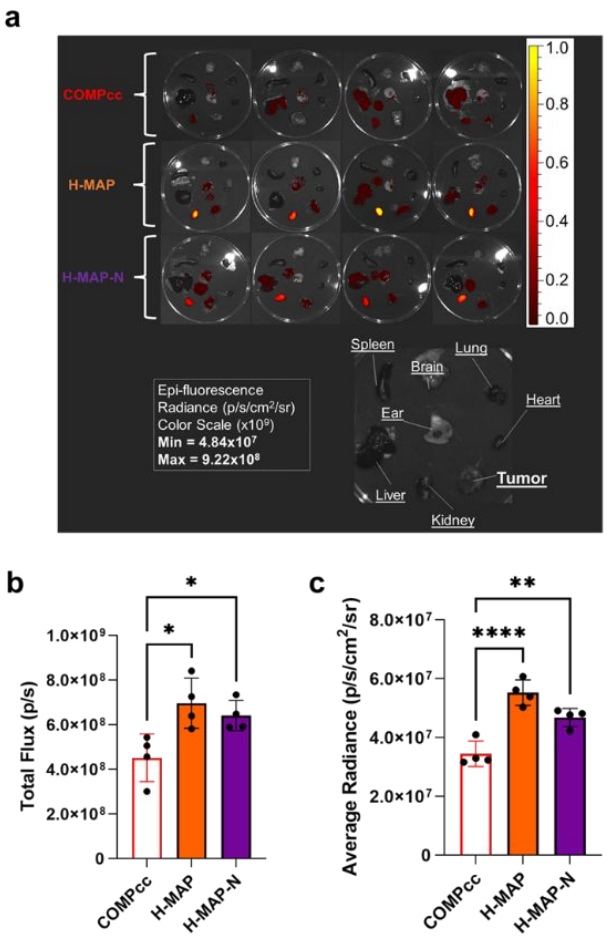

Figure 5 a. Ex vivo fluorescence biodistribution (630/680 nm ex/em) 30 min after injection of COMPcc, H-MAP, and H-MAP-N. Tumor fluorescence for each group is further shown in **b.** total photon flux (photon per second, p/s) and **c.** average radiance (photons per second per square centimeter per steradian, p/s/cm²/sr). * represents p-value<0.05, ** p-value < 0.01 , **** p-value < 0.0001 compared to COMPcc. Error bars represent standard deviation of four independent trials.

Conclusions

Design strategies to stabilize helical protein-protein interactions (PPI) have become an attractive method to generate therapeutics for large and relatively flat protein-protein interfaces[41]. Here, we show that multivalent assembled proteins (MAPs) can be employed for other helical targets by grafting critical PPI residues on the binding helix. We demonstrate this modularity by targeting the HIF1α C-TAD•p300 complex to generate HIF1α-MAPs (H-MAPs). The resulting H-MAP proteins show improved binding affinity to the p300 peptide, which translates to the ability to downregulate hypoxia-inducible genes *in vitro*, and the ability to localize in the hypoxic tumor microenvironment of TNBC cells within mice. H-MAPs thus show potential as a targeting modality that may be implemented for a diagnostic or therapeutic system. This is especially promising in comparison to previous HIF1α PDM binding affinities and current commercially available antibodies which also typically have lower binding affinities and cannot usually be produced in low cost, rapid growth *E. coli* expression systems[42-44]. Future design of MAPs may benefit from studying the design of more universally favorable linker and binding sequences to accommodate the engraftment of a variety of short helical sequences such as HIF1α C-TAD. This proof-of-concept design demonstrates the ability to use MAPs as a mix-and-match system for fusion design of PDMs utilizing other helical proteins involved in PPIs.

Author Contributions

CRediT authorship contribution statement: **Jin Kim Montclare**: Conceptualization, Funding acquisition, Formal analysis, Writing – review & editing. **Youssef Z. Wadghiri**: Conceptualization, Funding acquisition, Formal analysis, Writing – review & editing. **Dustin Britton**: Conceptualization, Data curation, Formal Analysis, Investigation, Methodology, Software, Visualization, Writing – original draft, Writing – review & editing. **Olga Katara:** Investigation, Software Analysis, Visualization, Data curation. **Chengliang Liu**: Data curation. **Sihan Jia**: Data curation. **Orin Mishkit**: Investigation, Software Analysis, Visualization, Data curation. **Andrew Wang:** Data curation. **Neelam Pandya:** Investigation, Data curation. **Heather Mao:** Investigation, Data curation. **Jakub Legocki:** Data curation. **Yingixn Xiao:** Data curation. **Orlando Aristizabal:** Data curation. **Deven Paul:** Data curation. **Yan Deng**: Data curation. **Robert Schneider:** Resources, Investigation, Funding.

Conflicts of interest

There are no conflicts to declare.

Acknowledgements

Funding. This work was supported by NSF-DMREF under Award Number DMR 1728858 and in part by NSF-DMR 2326688. Part of this work was performed at the NYU Grossman School Medicine Preclinical Imaging Laboratory, a shared resource partially supported by the NIH/SIG 1S10OD018337-01, the Laura and Isaac Perlmutter Cancer Center Support Grant, NIH/NCI 5P30CA016087, and the NIBIB Biomedical Technology

This journal is © The Royal Society of Chemistry 20xx

Please do not adjust margins

Resource Center Grant NIH P41 EB017183. This work was partially supported by the NYU Shifrin Myers Breast Cancer Discovery Fund (SMBCDF).

Notes and references

1. D. Rosenblum, N. Joshi, W. Tao, J. M. Karp and D. Peer, *Nature Communications*, 2018, **9**, 1410.
2. R. Jia, L. Teng, L. Gao, T. Su, L. Fu, Z. Qiu and Y. Bi, *Int J Nanomedicine*, 2021, **16**, 1525-1551.
3. L. Li, J. Wang, H. Kong, Y. Zeng and G. Liu, *Sci Technol Adv Mater*, 2018, **19**, 771-790.
4. Y. Li, L. Zhao and X. F. Li, *Technol Cancer Res Treat*, 2021, **20**, 15330338211036304.
5. G. M. Burslem, H. F. Kyle, A. Nelson, T. A. Edwards and A. J. Wilson, *Chemical Science*, 2017, **8**, 4188-4202.
6. J. Wei, Y. Yang, M. Lu, Y. Lei, L. Xu, Z. Jiang, X. Xu, X. Guo, X. Zhang, H. Sun and Q. You, *Mini-Reviews in Medicinal Chemistry*, 2018, **18**, 296-309.
7. V. Azzarito, K. Long, N. S. Murphy and A. J. Wilson, *Nat Chem*, 2013, **5**, 161-173.
8. P. M. Cromm, J. Spiegel and T. N. Grossmann, *ACS Chemical Biology*, 2015, **10**, 1362-1375.
9. A. Glas, D. Bier, G. Hahne, C. Rademacher, C. Ottmann and T. N. Grossmann, *Angew Chem Int Ed Engl*, 2014, **53**, 2489-2493.
10. J. A. Miles, D. J. Yeo, P. Rowell, S. Rodriguez-Marin, C. M. Pask, S. L. Warriner, T. A. Edwards and A. J. Wilson, *Chem Sci*, 2016, **7**, 3694-3702.
11. M. Pelay-Gimeno, A. Glas, O. Koch and T. N. Grossmann, *Angew Chem Int Ed Engl*, 2015, **54**, 8896-8927.
12. X. Qin, H. Chen, L. Tu, Y. Ma, N. Liu, H. Zhang, D. Li, B. Riedl, D. Bierer, F. Yin and Z. Li, *Journal of Medicinal Chemistry*, 2021, **64**, 13693-13703.
13. L. K. Henchey, S. Kushal, R. Dubey, R. N. Chapman, B. Z. Olenyuk and P. S. Arora, *Journal of the American Chemical Society*, 2010, **132**, 941-943.
14. B. B. Lao, I. Grishagin, H. Mesallati, T. F. Brewer, B. Z. Olenyuk and P. S. Arora, *Proc Natl Acad Sci U S A*, 2014, **111**, 7531-7536.
15. S. Kushal, B. B. Lao, L. K. Henchey, R. Dubey, H. Mesallati, N. J. Traaseth, B. Z. Olenyuk and P. S. Arora, *Proc Natl Acad Sci U S A*, 2013, **110**, 15602-15607.
16. J. P. Landry, Y. Ke, G. L. Yu and X. D. Zhu, *J Immunol Methods*, 2015, **417**, 86-96.
17. D. Britton, K. Punia, F. Mahmoudinobar, T. Tada, X. Jiang, P. D. Renfrew, R. Bonneau, N. R. Landau, X.-P. Kong and J. K. Montclare, *Biochemical Engineering Journal*, 2022, **187**, 108596.
18. R. Yan, Y. Zhang, Y. Li, L. Xia, Y. Guo and Q. Zhou, *Science*, 2020, **367**, 1444-1448.
19. A. Leaver-Fay, M. Tyka, S. M. Lewis, O. F. Lange, J. Thompson, R. Jacak, K. Kaufman, P. D. Renfrew, C. A. Smith, W. Sheffler, I. W. Davis, S. Cooper, A. Treuille, D. J. Mandell, F. Richter, Y. E. Ban, S. J. Fleishman, J. E. Corn, D. E. Kim, S. Lyskov, M. Berrondo, S. Mentzer, Z. Popovic, J. J. Havranek, J. Karanicolas, R. Das, J. Meiler, T. Kortemme, J. J. Gray, B. Kuhlman, D. Baker and P. Bradley, *Methods Enzymol*, 2011, **487**, 545-574.
20. Pymol, The PyMOL Molecular Graphics System, Version 2.0 Shrödinger, LLC.
21. J. Lan, J. Ge, J. Yu, S. Shan, H. Zhou, S. Fan, Q. Zhang, X. Shi, Q. Wang, L. Zhang and X. Wang, *bioRxiv*, 2020, DOI: 10.1101/2020.02.19.956235, 2020.2002.2019.956235.
22. F. DiMaio, A. Leaver-Fay, P. Bradley, D. Baker and I. André, *PLoS One*, 2011, **6**, e20450.
23. R. F. Alford, A. Leaver-Fay, J. R. Jeliazkov, M. J. O'Meara, F. P. DiMaio, H. Park, M. V. Shapovalov, P. D. Renfrew, V. K. Mulligan, K. Kappel, J. W. Labonte, M. S. Pacella, R. Bonneau, P. Bradley, R. L. Dunbrack, Jr., R. Das, D. Baker, B. Kuhlman, T. Kortemme and J. J. Gray, *J Chem Theory Comput*, 2017, **13**, 3031-3048.
24. L. Yin, A. S. Agustinus, C. Yuvienco, T. Minashima, N. L. Schnabel, T. Kirsch and J. K. Montclare, *Biomacromolecules*, 2018, **19**, 1614-1624.
25. S. K. Gunasekar, M. Asnani, C. Limbad, J. S. Haghpanah, W. Hom, H. Barra, S. Nanda, M. Lu and J. K. Montclare, *Biochemistry*, 2009, **48**, 8559-8567.
26. A. Alard, O. Katsara, T. Rios-Fuller, C. Parra, U. Ozerdem, A. Ernlund and R. J. Schneider, *Cell Rep*, 2023, **42**, 112646.
27. L. G. Nivón, R. Moretti and D. Baker, *PLoS One*, 2013, **8**, e59004.
28. J. W. Lee, J. Ko, C. Ju and H. K. Eltzschig, *Experimental & Molecular Medicine*, 2019, **51**, 1-13.
29. S. Y. Lau, A. K. Taneja and R. S. Hodges, *J Biol Chem*, 1984, **259**, 13253-13261.
30. S. C. Kwok and R. S. Hodges, *J Biol Chem*, 2004, **279**, 21576-21588.
31. N. E. Shepherd, H. N. Hoang, G. Abbenante and D. P. Fairlie, *J Am Chem Soc*, 2009, **131**, 15877-15886.
32. N. J. Greenfield, *Nat Protoc*, 2006, **1**, 2876-2890.
33. S. W. Provencher and J. Glockner, *Biochemistry*, 1981, **20**, 33-37.
34. N. Sreerama, S. Y. Venyaminov and R. W. Woody, *Protein Sci*, 1999, **8**, 370-380.
35. I. Nyqvist and J. Dogan, *Scientific Reports*, 2019, **9**, 16557.
36. D. Britton, C. Liu, S. Jia, D. Paul, J. Legocki, Y. Xiao, X. Jiang, X.-P. Kong and J. K. Montclare, *Biochemical Engineering Journal*, 2024, **205**, 109261.
37. X. Yu, C. N. Pegram, D. D. Bigner and V. Chandramohan, *J Immunol Methods*, 2017, **442**, 49-53.
38. A. Inoue, T. Yasuda, B. Zhu, T. Kitaguchi, A. Murakami and H. Ueda, *Scientific Reports*, 2021, **11**, 22590.
39. C. Zer, K. N. Avery, K. Meyer, L. Goodstein, K. P. Bzymek, G. Singh and J. C. Williams, *Protein Eng Des Sel*, 2017, **30**, 409-417.
40. P. Yazaki, T. Lwin, M. Minnix, L. Li, A. Sherman, J. Molnar, A. Miller, P. Frankel, J. Chea, E. Poku, N. Bowles, R. Hoffman, J. Shively and M. Bouvet, *J Biomed Opt*, 2019, **24**, 1-9.
41. A. M. Watkins, T. W. Craven, P. D. Renfrew, P. S. Arora and R. Bonneau, *Structure*, 2017, **25**, 1771-1780.e1773.
42. N. K. Tripathi and A. Shrivastava, *Frontiers in Bioengineering and Biotechnology*, 2019, **7**.
43. N. B. Mohammed, M. A.-H. Ahmed, S. B. Roop, M. M. A. Mohamed, *, A. I. R. Hassan, S. S. Kulvinder, A. B. Nabih and M. R. Elrashdy, *J. Microbiol. Biotechnol.*, 2015, **25**, 953-962.
44. S. K. Gupta and P. Shukla, *Critical Reviews in Biotechnology*, 2016, **36**, 1089-1098.

This journal is © The Royal Society of Chemistry 20xx